Iranian Journal of Materials Forming 13 (4) (2026) 15-23

Online ISSN: 2383-0042

IJMF

Iranian Journal of Materials Forming

Journal Homepage: http://ijmf.shirazu.ac.ir

Research Article

Influence of Pre-Aging on Microhardness and Corrosion Resistance of AA6061 Processed by ECAP and NECAP

Arman Hasani* and Abdelhameed Fardosi

Department of Mechanical Engineering, Faculty of Engineering, University of Kurdistan, Sanandaj 15175-66177, Iran

ARTICLE INFO

Article history:

Received: 9 February 2026
Reviewed: 12 March 2026
Revised: 10 May 2026
Accepted: 31 May 2026

Keywords:

Aluminum alloy
SPD
Ultrafine-grained materials
Corrosion
Hardness

Please cite this article as:

Hasani, A., & Fardosi, A. (2026). Influence of pre-aging on microhardness and corrosion resistance of AA6061 processed by ECAP and NECAP. *Iranian Journal of Materials Forming*, *13*(4), 15-23. https://doi.org/10.22099/IJMF.2026.55621.1372

ABSTRACT

This study investigates the initial heat treatment, namely annealing versus the peak-aged T6 condition, and subsequent severe plastic deformation (SPD) via equal-channel angular pressing (ECAP) and non-equal-channel angular pressing (NECAP), on the microhardness and corrosion resistance of AA6061 aluminum alloy. Samples in both the annealed and peak-aged conditions were subjected to a single pass of ECAP or NECAP, respectively. Microhardness was characterized using Vickers measurements on planes oriented perpendicular to the pressing (PPD) and extrusion (PED) directions. Corrosion behavior was evaluated using electrochemical impedance spectroscopy (EIS) conducted in a 3.5% NaCl solution. The results revealed that initial peak-aging substantially enhanced hardness while concurrently diminishing corrosion resistance relative to the annealed state. Both ECAP and NECAP processing resulted in significant improvements in hardness and corrosion resistance for both initial material conditions. A comparison of the SPD routes indicated that NECAP yielded slightly higher hardness values, particularly for the peak-aged material, whereas ECAP provided superior hardness uniformity between the PPD and PED planes and slightly enhanced corrosion resistance. Notably, the beneficial impact of SPD processing on hardness (relative increase) and corrosion resistance (final attained value) was more pronounced for the material initially in the annealed condition. These findings highlight the significant interplay between the initial microstructure and the chosen SPD methodology in tailoring the resultant mechanical and electrochemical characteristics of the AA6061 alloy.

1. Introduction

During the last two decades, severe plastic deformation has attracted increasing attention from scientists for its potential to create ultrafine-grained and nanostructured bulk materials. Numerous advantages of SPD operations have attracted experts' interest in the characterization, development, and creation of new SPD processes [1]. A few of them are equal-channel angular pressing, equal-channel angular rolling (ECAR), parallel tubular channel angular pressing (PTCAP), cyclic closed die forging (CCDF), and constrained groove pressing (CGP). ECAP has been widely used among SPD operations;

* Corresponding author
E-mail address: a.hasani@uok.ac.ir (A. Hasani)
https://doi.org/10.22099/IJMF.2026.55621.1372

however, achieving very large strains requires repeating the process, which is one of its disadvantages. Large strains can be achieved if the process is carried out under non-equal-channel angular pressing (NECAP) without repetition of the process, resulting in a higher equivalent von Mises strain than ECAP (1.44 versus 1.15, respectively) [3]. Due to the advantages of NECAP, the process has attracted increasing attention from researchers [4, 5].

Aluminum alloys, for example, Al6061, are of immense industrial importance and have a wide range of application due to their important properties, such as, light weight, high electrical as well as thermal conductivity, resistance against corrosion, and ductility. Therefore, they are used for consumer items, military applications, and the shipping industry. Aluminum is lighter than iron and other conventional metals, making it widely used in the aerospace and aircraft industries. Each kilogram of weight reduction translates into greater fuel savings and enhanced payload. Moreover, aluminum is easily machinable, castable, extrudable, and rollable, and most of its alloys are age-hardenable [6].

Khanlari and co-authors [2] investigated the effect of the NECAP process on hardness and microstructure of Al6061, reporting that the average hardness improved by 38.3%, from 55.1 HV to 76.2 HV. Mohamed Ibrahim and his team [7] conducted a study on the effect of ECAP on microstructure development and mechanical properties of Al6061 alloy specimens that were pre-annealed for analysis. The average microhardness improved by 15.2%, 21.8%, and 27.3% for 1, 2, and 4 passes of ECAP, respectively.

Experiments by Nejadseyfi and his colleagues [8] were designed to investigate the synergistic influence of pre-deformation heat treatment and ECAP on AA6061 corrosion behavior. The results showed that increasing the number of ECAP led to a decrease in I_{corr} values.

Mehdizade and co-authors [9] investigated the influence of ECAP and aging on the surface grain structure, as well as the corrosion behavior, of AA6063. They performed a maximum of six passes of ECAP with aging at 180 °C for 8 h. The grain size was observed to decrease with increasing ECAP pass number, whereas a decrease in secondary-phase particle size was accompanied by an increase in precipitate density. With an increasing number of ECAP passes, resistance against corrosion improved, as supported by decreased weight loss on immersion tests.

In other research by Rominiyi and co-authors [10], studied the effects of post-ECAP aging on peak-aged 6061 aluminum alloy. It was observed that grain refinement was the major factor responsible for the increase in hardness, as well as the formation of dislocation networks at grain boundaries and within grains.

Despite these valuable investigations, the combined influence of pre-aging and SPD processing routes such as ECAP and NECAP on hardness and corrosion resistance of AA6061 remains insufficiently understood. While SPD offers substantial mechanical improvements through grain refinement and work hardening, its effect on corrosion resistance is critical for practical applications of AA6061 in aerospace, automotive, and marine environments. The principal objective of this work is therefore to investigate the effect of pre-aging on both hardness and corrosion resistance of AA6061 specimens subjected to ECAP and NECAP processing routes, providing a better understanding of the processing-structure-property relations in SPD-processed aluminum alloys.

2. Experimental Procedure

2.1. Initial samples

AA6061 alloy samples were prepared in six groups with different thermomechanical conditions, as summarized in Table 1. All samples were machined to a length of 50 mm length and a 10×10 mm² cross-section prior to SPD processing.

2.2. NECAP and ECAP processes

In the present study, a single pass was intentionally applied to both ECAP and NECAP to ensure a direct comparison between the two routes under matched processing conditions. Since NECAP inherently produces a higher strain in a single pass due to its reduced exit-channel cross-section, repeated passes are

Table 1. Sample designations and corresponding processing conditions

Sample code	Initial condition	Heat treatment details	SPD process	Final condition
A	Ac-received	413 °C, 5 h	-	Annealed
A-E	Annealed	-	ECAP (1 pass)	Annealed + ECAP
A-N	Annealed	-	NECAP (1 pass)	Annealed + NECAP
T6	Annealed	527 °C, 30 min → water quench → 160 °C, 18 h	-	Peak-aged
T6-E	Peak-aged	-	ECAP (1 pass)	Peak-aged + ECAP
T6-N	Peak-aged	-	NECAP (1 pass)	Peak-aged + NECAP

not part of its standard practical concept; therefore, the comparison was limited to one pass for each route. The corresponding effective strains are approximately 1.15 for ECAP and 1.44 for NECAP, as reported in the introductory section.

Both ECAP and NECAP were conducted using square-sectioned 90° dies with square channels and a constant extrusion punch velocity of 3 mm/min. The die geometry represented the main difference between the two processes: for ECAP, a constant cross-section of 10×10 mm² was used throughout both the entry channel and the exit channel, whereas for NECAP, the exit channel width was reduced to 5 mm. The lubricant employed was MoS_2 grease for both treatments, with all tests conducted at room temperature.

Although the temperature during pressing was not directly measured, the low punch speed (3 mm/min) and the use of MoS_2 lubricant indicate that frictional and adiabatic heating were limited and are unlikely to have significantly affected the aging state established at 160 °C.

2.3. Corrosion tests

Corrosion tests were conducted on small specimens cut from the center of each sample. The corrosion behavior of the samples was studied using electrochemical impedance spectroscopy (EIS). Electrochemical tests were performed at room temperature in a 3.5% NaCl solution, with the specimen acting as the working electrode, an Ag/AgCl reference electrode, and a platinum rod as the auxiliary electrode. The frequency range for EIS measurements was 10^{-1} to 10^{5} Hz, with an amplitude voltage of 10 mV.

2.4. Hardness measurement

Some researchers suggested cutting the samples across the pressing direction of pressing (PPD) [11, 12], whereas others suggested that they be cut across the extrusion direction (PED) [2], as shown in Fig. 1.

As shown in Fig. 1, a portion of the deformed region of the specimens obtained from each process was used for hardness testing. In these specimens, two distinct planes were considered. The first plane was cross-sectioned at the center to examine the surface oriented perpendicularly to the pressing direction (PPD), while the second plane was cross-sectioned to examine the surface oriented perpendicularly to the extrusion direction (PED). Vickers microhardness measurements were subsequently performed at four points on each plane (marked as red circles), located within the central deformed region to ensure representative data.

3. Results and Discussion

3.1. Hardness tests

It is worth noting that the hardness measured in the ECAP/NECAP-processed specimens may be governed by the deformation route and die geometry, which in turn determine the local strain distribution and the resulting microstructural anisotropy.

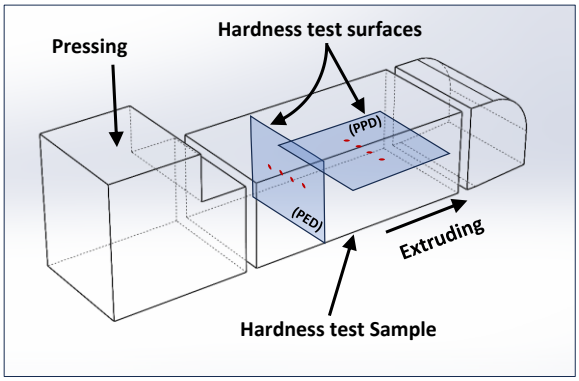

Fig. 1. Schematic illustration of the deformed specimen, showing the surfaces (PPD and PED) and the locations (red circles) of the Vickers microhardness measurements.

In the present work, hardness was measured on the mid-plane of the central deformed region to obtain a more representative value of the bulk response and to minimize the influence of surface friction and local strain heterogeneity. These measurements were conducted within the central deformed region of the specimens to confirm the uniformity of deformation and ensure that the plane strain conditions were successfully established across the cross-sections.

The variations between individual points were negligible and could be considered insignificant, which is consistent with the establishment of plane strain conditions in the applied processes and justifies the use of the arithmetic mean as a representative indicator of the material's hardness. Consequently, a shift in the measurement plane would be expected to produce different hardness values. Fig. 2 depicts the results of the hardness measurements. It presents the hardness values of the PPD and PED surfaces for the ECAP and NECAP operations in two separate graphs, along with the hardness of the base samples in both annealed and peak-aged conditions. The sample labels in Fig. 2 correspond to the codes defined in Table 1. Notably, the reported hardness values in each plot represent the arithmetic average of four distinct measurements performed on the corresponding plane, as illustrated in Fig. 1.

Fig. 2 displays the evolution of hardness for the material under various initial heat treatments after ECAP (Fig. 2(a)) and NECAP (Fig. 2(b)). As observed, the processing route and initial heat treatment state had a noticeable effect on the hardness response of the specimens.

The initial hardness measurements reveal the significant impact of the pre-processing heat treatment. The 'Annealed' specimens had a low baseline hardness of 40.46 HV, indicating a soft starting point. The 'Peak-aged' specimens had a much higher initial hardness of 83.72 HV. This confirms that the peak-aging heat treatment significantly hardened the material before it was deformed, presumably through the development of fine precipitates, so that the peak-aged material was initially about 107% harder than the annealed counterpart.

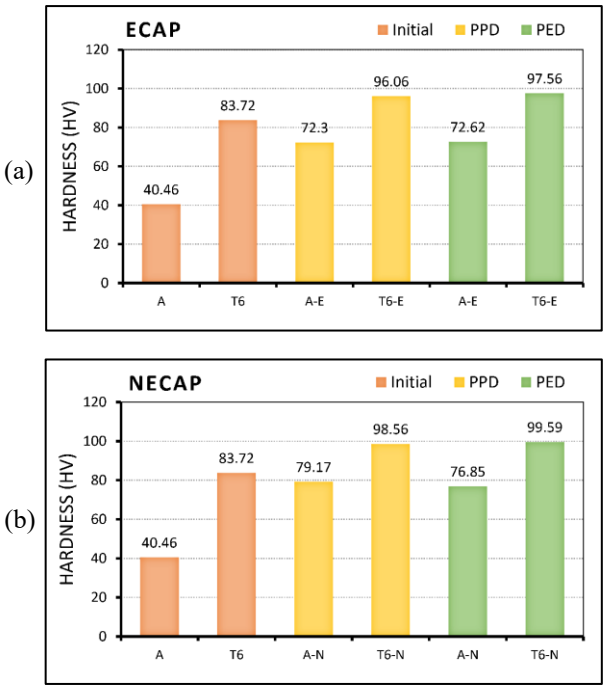

Fig. 2. Comparison of hardness values for the two initial conditions on PPD and PED surfaces (as indicated in Fig. 1), before and after (a) ECAP and (b) NECAP processing. Note: Each data point represents the arithmetic average of four measurements per plane.

Observing the impact of ECAP processing (Fig. 2(a)), subjecting the annealed material to ECAP led to a remarkable hardness improvement in hardness due to work hardening. Hardness increased to 72.3 HV on the PPD plane and to 72.62 HV on the PED plane, reflecting improvements of 78.7% and 79.5%, respectively, compared with the as-annealed state. The similarity of these values indicates fairly consistent hardening between the two planes for this condition. With the application of ECAP to the peak-aged material, hardness increased further to 96.06 HV (PPD) and 97.56 HV (PED). The relative improvement, however, was significantly lower (14.7% and 16.5%, respectively) compared to the initially annealed material. Notably, ECAP processing resulted in extremely uniform hardness between the PPD and PED planes for both the initial states, with differences being less than 0.5 HV.

Fig. 2(b) shows the hardness development after NECAP processing. Like ECAP, NECAP significantly enhanced the hardness of the originally annealed material. The hardness of the PPD plane was 79.17 HV (95.7% increase) and the PED plane was 76.85 HV

(89.9% increase). This is a dramatic hardening effect, with the percentage increases being very significant. When applied to the peak-aged material, NECAP further increased hardness to 98.56 HV (PPD, +17.7%) and 99.59 HV (PED, +19.0%). These values represent the highest absolute hardness levels observed across all conditions tested. Again, consistent with the ECAP results, the percentage gain was relatively modest compared to the initially annealed material. Unlike the high uniformity seen with ECAP, NECAP processing resulted in slightly larger, though still minor, variations between the planes. For the annealed + NECAP sample, the PPD plane was slightly harder (~2.3 HV difference), whereas for the peak-aged + NECAP sample, the PED plane exhibited slightly greater hardness (~1 HV difference).

The obtained results indicate a strong dependence on both the initial material condition and the specific severe plastic deformation (SPD) technique applied. Employing peak-aged material as the starting condition invariably results in substantially greater final hardness following both ECAP and NECAP processing, compared with annealed material. This observation underscores the contribution of precipitation hardening inherited from the initial thermal treatment. Nevertheless, the relative increase in hardness attributed to the deformation process itself (work hardening) is considerably more pronounced when processing the initially softer, annealed material. This implies that although the pre-existing hardness in the peak-aged condition restricts the potential percentage gain achievable through subsequent work hardening, the annealed condition presents a greater capacity for relative strengthening induced by the deformation. Fundamentally, the hardness improvement observed following both ECAP and NECAP processing is attributed to the microstructural evolution induced by severe plastic deformation. This primarily involves significant grain refinement and the generation of a high density of dislocation networks, situated both at grain boundaries and within the refined grain interiors [10].

In comparing the two SPD processes, NECAP generally resulted in slightly greater hardening than ECAP when processing the annealed material. This difference was particularly evident on the PPD plane. For the peak-aged starting material, both processes achieved high levels of hardness; however, NECAP again produced slightly higher final hardness values and marginally greater percentage hardness gains compared to ECAP. Overall, under the experimental conditions employed, NECAP processing exhibited a tendency to yield slightly higher final hardness relative to ECAP for both initial material conditions investigated.

Furthermore, the hardness uniformity varied between the two processes. ECAP processing yielded highly uniform hardness between the PPD and PED planes for both initial states (< 0.5 HV difference). In contrast, NECAP processing exhibited slightly larger, although still minor, variations between these planes (~1-2.3 HV difference). This observation could imply minor variations in the homogeneity of the strain distribution or the resulting texture evolution characteristic of the NECAP process relative to ECAP, consequently influencing these specific planes differently.

The increase in hardness observed after ECAP and NECAP is consistent with the combined action of precipitation strengthening in the peak-aged condition and grain refinement/ dislocation strengthening induced by severe plastic deformation. In particular, the higher initial hardness of the peak-aged specimens can be attributed to their heat-treatment state, while the additional hardening after SPD is in line with the expected contribution of dislocation accumulation and grain refinement. Although direct measurements of precipitate spacing and dislocation density were not performed, the observed trends are consistent with the established response of AA6061 under SPD and aging conditions.

In summary, commencing with peak-aged material establishes a substantially harder initial condition, ultimately resulting in the highest final hardness values after SPD processing. However, the relative strengthening attained via work hardening during both ECAP and NECAP processing, attributed to the previously mentioned mechanisms involving grain refinement and dislocation density increase [10], is greatest when beginning with the initially softer,

annealed material. Under the investigated conditions, NECAP proved marginally more effective than ECAP in attaining the highest absolute hardness, whereas ECAP provided slightly superior hardness homogeneity between the examined planes.

In closing, it should be noted that, taking into account the specific hardness-testing conditions employed in the present work, together with the peak-aged state of the investigated specimens, the reported hardness values should be interpreted within this particular experimental context. Since most previously published studies on similar aluminum alloys have been carried out under different aging conditions and under different measurement configurations, the present results cannot be directly compared with those of earlier works.

3.2. Corrosion tests

The corrosion behavior of the aluminum alloy under the various thermomechanical conditions was examined using electrochemical impedance spectroscopy (EIS). The analysis of the acquired EIS measurements involved fitting the experimental data to the equivalent electrical circuit (EEC) depicted in Fig. 3. This procedure followed the model detailed in [13] and was carried out using the ZView software package. The selected EEC model accounts for the distinct electrochemical phenomena that occur at the metal/ electrolyte interface.

The circuit elements represent: R_{sol} (NaCl solution resistance), Rf (resistance of the passive oxide film), and Rct (charge transfer resistance, indicative of the corrosion rate). Constant phase elements, CPE_f and CPE_{dl}, were employed instead of pure capacitances to model the non-ideal behavior of the oxide film and the electrical double layer, respectively. Considering the system's non-ideal nature, the CPE is mathematically described by the following relation [14]:

$$Z_{\mathrm{CPE}} = \frac{1}{\mathrm{Y}_0(j\omega)^{\mathrm{n}}} \tag{1}$$

Within this expression, Z_{CPE} denotes the impedance of the constant phase element (CPE), Y_0 represents the admittance corresponding to an ideal capacitance, j signifies the imaginary unit ($\sqrt{-1}$), and ω indicates the angular frequency ($2\pi f$). The key parameter, n, is a dimensionless value ranging between 0 and 1 that quantifies the degree of deviation from ideal capacitive behavior. The CPE behaves as a resistor for n = 0 and as an ideal capacitor for n = 1.

RL (resistance to induction) and L (inductance) are related to the pitting corrosion by the following relation:

$$\frac{1}{R_p} = \frac{1}{R_{\mathrm{film}} + R_t} + \frac{1}{R_{\mathrm{adsorption}}} \tag{2}$$

The characteristic Nyquist plots derived from the EIS measurements for all samples are presented in Fig. 4.

The values of the corresponding electrochemical parameters, determined by fitting these EIS data to the EEC in Fig. 3, are compiled in Table 2.

Key parameters considered in the present analysis include Rf, Rct, and the total polarization resistance (Rp), the latter providing a general indication of the material's resistance to corrosion under the specified test conditions. Within the Nyquist plot representation, an

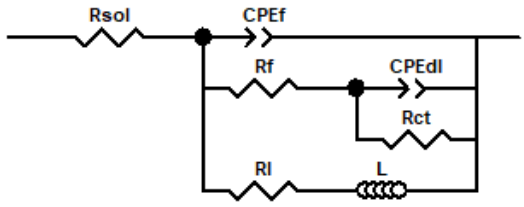

Fig. 3. The equivalent circuit used to fit EIS diagrams.

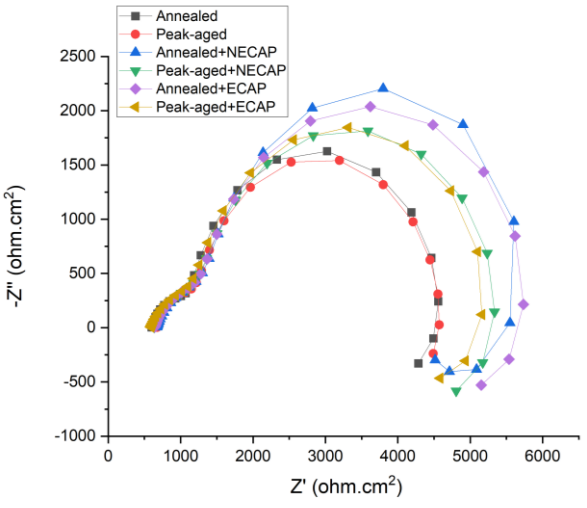

Fig. 4. Nyquist plots of all samples.

Table 2. Electrochemical parameters obtained from EIS fitting using the equivalent circuit for AA6061 samples

Samples / Parameters	Annealed	Peak-aged	Annealed + NECAP	Peak-aged + NECAP	Annealed + ECAP	Peak-aged + ECAP
Rsol (Ω.cm²)	597.4	673.2	669.2	632.5	639.3	586.3
CPEf-Y_0 (F.cm^{-2})	1.09×10^{-5}	9.24×10^{-6}	1.76×10^{-5}	1.73×10^{-5}	1.65×10^{-5}	1.78×10^{-5}
CPEf-n	0.76	0.8	0.69	0.68	0.69	0.69
Rf (Ω.cm²)	772.1	821.7	1198	1104	1131	1031
CPEdl-Y_0 (F.cm^{-2})	2.20×10^{-5}	2.15×10^{-5}	1.54×10^{-5}	1.48×10^{-5}	1.54×10^{-5}	1.71×10^{-5}
CPEdl-n	0.98	0.97	0.97	0.97	0.97	0.97
Rct (Ω.cm²)	3415	3200	5345	4109	4596	4159
RL (Ω.cm²)	11423	9258	8800	9625	11707	10617
L (H.cm²)	27217	46623	5332	20692	20796	16663
Rp (Ω.cm²)	3063.993	2803.745	3752.747	3381.529	3845.703	3485.939

increased diameter of the capacitive semicircle is generally associated with a higher charge transfer resistance (Rct) and, consequently, enhanced corrosion resistance [13, 15]. Although aluminum inherently develops a protective passive oxide film, its known susceptibility to pitting corrosion when exposed to chloride-containing environments, resulting from localized breakdown of this oxide film, constitutes a critical consideration.

A comparison of the baseline samples (Table 2) reveals that the annealed condition demonstrates greater corrosion resistance relative to the peak-aged condition prior to the application of severe plastic deformation (SPD). The polarization resistance (Rp) determined for the annealed sample (3063.993 Ω.cm²) is substantially higher than the value obtained for the peak-aged sample (2803.745 Ω.cm²). This trend is also reflected in the charge transfer resistance (Rct), for which values of 3415 Ω.cm² and 3200 Ω.cm² were measured for the annealed and peak-aged states, respectively.

This finding suggests that the peak-aging treatment, while enhancing mechanical properties through precipitation hardening in alloys such as AA6061, concurrently degrades corrosion resistance. Based on the well-documented phase composition of AA6061 in the literature [16], it is suggested that the formation of precipitates (e.g., Mg_2Si, AlFeSi) during peak-aging may introduce electrochemical heterogeneity. These second-phase particles could potentially act as local cathodes or anodes relative to the aluminum matrix, which is often associated with the establishment of microscopic galvanic cells that accelerate corrosion processes, particularly pitting [8, 9, 16].

Direct phase identification by EDS or XRD was not performed in this study. The discussion of precipitate-induced galvanic effects is based on the known phase composition of AA6061 from the literature [16].

Regarding the influence of deformation on corrosion resistance, it can be observed that subsequent application of SPD via either NECAP or ECAP resulted in a substantial improvement in corrosion resistance for both initial material states, as evidenced by the parameters presented in Table 2.

For the initially annealed material, Rp increased markedly from approximately 3064 Ω.cm² to ~3753 Ω.cm² (NECAP) and ~3846 Ω.cm² (ECAP). Rct also exhibited a large increase, particularly following NECAP processing (from 3415 Ω.cm² to 5345 Ω.cm²).

Similarly, for the initially peak-aged material, Rp increased from approximately 2804 Ω.cm² to ~3382 Ω.cm² (NECAP) and ~3486 Ω.cm² (ECAP), with corresponding increases observed in Rct (from 3200 Ω.cm² to the range of ~4109-4159 Ω.cm²).

This enhancement is consistent with the microstructural refinement typically associated with SPD processes, which commonly involves grain-size

reduction and an increased dislocation density. Such modifications may facilitate the formation of a more homogeneous and potentially more protective passive film. Furthermore, SPD processes may induce fragmentation and redistribution of second-phase precipitates, potentially reducing the intensity of localized galvanic effects compared with the coarser precipitate structure present in the as-aged condition [8, 9].

It should be noted that the present work did not include direct microstructural observations by OM or FESEM; therefore, the discussion of grain morphology, precipitate redistribution, and passive-film features is interpreted indirectly from the measured corrosion response and from previously reported behavior of AA6061 processed under similar conditions. Accordingly, the present conclusions regarding microstructural evolution should be regarded as consistent with the electrochemical results and the available literature rather than as direct microstructural evidence.

Therefore, comparing the two SPD techniques, ECAP processing yielded slightly higher polarization resistance (Rp) values relative to NECAP for both the initially annealed (3846 vs. 3753 Ω.cm²) and peak-aged (3486 vs. 3382 Ω.cm²) conditions. Based on the Nyquist plot analysis, the difference between NECAP and ECAP could be considered less pronounced for the peak-aged samples, with both methods resulting in significant improvement. For the annealed samples, the higher Rp value observed following ECAP suggests slightly better overall corrosion resistance; however, the higher Rct value measured after NECAP might indicate subtle differences in the dominant resistance mechanism or the characteristics of the passive film induced by the distinct strain paths associated with the two methods.

4. Conclusion

In the present study, the influence of initial aging and subsequent severe plastic deformation (ECAP and NECAP) on the hardness (measured on PPD and PED planes) and corrosion behavior of AA6061 alloy was investigated. The interplay between the initial aging state and the deformation path leads to the following insights:

1) Saturation of work hardening: Peak-aging prior to SPD increases initial hardness by approximately 107% but reduces the efficiency of subsequent hardening via SPD from ~79% (annealed) to only ~16%, revealing a saturation limit imposed by pre-existing precipitates.
2) Strain path vs. hardness isotropy: While NECAP achieves higher absolute hardness (+2-3 HV), it induces measurable anisotropy between the PPD and PED planes (ΔHV ≈ 1-2.3). In contrast, ECAP results in near-perfect isotropy (ΔHV < 0.5), suggesting that deformation geometry controls textural homogeneity.
3) Corrosion depends on homogeneity, not strain magnitude: Despite NECAP's higher imposed strain, ECAP delivers slightly better corrosion resistance (Rp: 3846 vs. 3753 Ω.cm² for annealed condition), demonstrating that uniform strain distribution and passive film formation outweigh accumulated strain.
4) Persistent galvanic heterogeneity: Peak-aged + SPD samples do not reach the corrosion resistance of annealed + SPD samples. This persistent difference confirms that precipitate-induced galvanic effects are not entirely eliminated by a single SPD pass.
5) Design guideline: The annealed + ECAP condition offers an optimize balance between hardness and corrosion resistance. In contrast, the peak-aged + NECAP condition maximizes absolute hardness but results in diminished corrosion resistance and isotropy.

Authors' contributions

A. Hasani: Conceptualization, Methodology, Resources, Investigation, Formal analysis, Writing original draft, Supervision, Project administration

A. Fardosi: Investigation, Formal analysis, Data curation, Review & editing

Conflict of interest

The authors declare that there is no conflict of interest regarding the publication of this manuscript.

Funding

The authors received no financial support for the research, authorship, and/ or publication of this article.

5. References

[1] Bagherpour, E., Pardis, N., & Reihanian, M. (2018). An overview on severe plastic deformation: Research status, techniques classification, microstructure evolution, and applications. *The International Journal of Advanced Manufacturing Technology*, *100*, 1647-1734. https://doi.org/10.1007/s00170-018-2652-z

[2] Khanlari, H., Honarpisheh, M. (2020). Investigation of microstructure, mechanical properties and residual stress in non-equal-channel angular pressing of 6061 aluminum alloy. *Transactions of the Indian Institute of Metals*, *73*(9), 1109-1121. https://doi.org/10.1007/s12666-020-01945-5

[3] Hasani, A., Toth, L. S., & Beausir, B. (2010). Principles of non-equal channel angular pressing. *Journal of Engineering Materials and Technology*, *132*(3), 0310001. https://doi.org/10.1115/1.4001261

[4] Toth, L. S., Lapovok, R., Hasani, A., & Gu, C. (2009). Non-equal channel angular pressing of aluminum alloy. *Scripta Materialia*, *61*(12), 1121-1124. https://doi.org/10.1016/j.scriptamat.2009.09.006

[5] Hasani, A., Toth, L. S., & Rouhani, S. M. (2019). A new flow line function for modeling material trajectory and textures in nonequal-channel angular pressing. *Advances in Materials Science and Engineering*, *2019*(1), 5682585. https://doi.org/10.1155/2019/5682585

[6] Khan, A. S., & Meredith, C. S. (2010). Thermo-mechanical response of Al6061 with and without equal channel angular pressing (ECAP). *International Journal of Plasticity*, *26*(2), 189-203. https://doi.org/10.1016/j.ijplas.2009.07.002

[7] El Aal, M. I. A. (2020). The influence of ECAP and HPT processing on the microstructure evolution, mechanical properties and tribology characteristics of an Al6061 alloy. *Journal of Materials Research and Technology*, *9*(6), 12525-12546. https://doi.org/10.1016/j.jmrt.2020.08.099

[8] Nejadsey, O., Shokuhfar, A., Dabiri, A., & Azimi, A. (2015). Combining equal-channel angular pressing and heat treatment to obtain enhanced corrosion resistance in 6061 aluminum alloy. *Journal of Alloys and Compounds*, *648*, 912-918. https://doi.org/10.1016/j.jallcom.2015.05.177

[9] Mehdizade, M., Eivani, A. R., & Soltanieh, M. (2020). Effects of reduced surface grain structure and improved particle distribution on pitting corrosion of AA6063 aluminum alloy. *Journal of Alloys and Compounds*, *838*, 155464. https://doi.org/10.1016/j.jallcom.2020.155464

[10] Rominiyi, A. L., Oluwasegun, K. M., Olawale, J. O., Shongwe, M. B., & Adetunji, A. R. (2021). Effect of post-ECAP aging on the microstructure, hardness and impact behavior of 6061 Al alloy. *Materials Today: Proceedings*, *38*, 1031-1034. https://doi.org/10.1016/j.matpr.2020.05.670

[11] Zheng, Z. J., Gao, Y., Gui, Y., & Zhu, M. (2012). Corrosion behavior of nanocrystalline 304 stainless steel prepared by equal channel angular pressing. *Corrosion Science*, *54*, 60-67. https://doi.org/10.1016/j.corsci.2011.08.049

[12] Minárik, P., Král, R., & Janeček, M. (2013). Effect of ECAP processing on corrosion resistance of AE21 and AE42 magnesium alloys. *Applied Surface Science*, *281*, 44-48. https://doi.org/10.1016/j.apsusc.2012.12.096

[13] Shishesaz, M. R., Ghobadi, M., Asadi, N., Zarezadeh, A., Saebnoori, E., Amraei, H., Schubert, J., & Chocholaty, O. (2021). Surface pretreatments of AA5083 aluminum alloy with enhanced corrosion protection for cerium-based conversion coatings application: Combined experimental and computational analysis. *Molecules*, *26*(24), 7413. https://doi.org/10.3390/molecules26247413

[14] Ezuber, H. (2008). A study on the corrosion behavior of aluminum alloys in seawater. *Materials & Design*, *29*(4), 801-805. https://doi.org/10.1016/j.matdes.2007.01.021

[15] Cao, C. (1990). On the impedance plane displays for irreversible electrode reactions based on the stability conditions of the steady-state—II. Two state variables besides electrode potential. *Electrochimica Acta*, *35*(5), 837-844. https://doi.org/10.1016/0013-4686(90)90078-E

[16] He, T., Shi, W., Xiang, S., Huang, C., & Ballinger, R. G. (2021). Influence of aging on corrosion behavior of the 6061 cast aluminum alloy. *Materials*, *14*(8), 1821. https://doi.org/10.3390/ma14081821